CrossMark

Preparation of nanocrystalline praseodymium oxide with different shapes via a simple thermal decomposition route

Sahar Zinatloo-Ajabshir[1] · Masoud Salavati-Niasari[1] · Masood Hamadanian[1]

Abstract Present report describes the surfactant-free synthesis and characterization of nanocrystalline praseodymium oxide. For this purpose, praseodymium source ([PrL(NO$_3$)$_2$]NO$_3$ (L = (N,N′-bis(2′-hydroxyacetophenon-imine)-o-dipropylene triamin) was prepared and its thermal decomposition was performed in at various temperatures in the 300–800 °C. Results of this investigation demonstrate that praseodymium oxide with very uniform sphere-like shape, small grain size and pure cubic phase could be synthesized by thermal decomposition of the obtained praseodymium source at 600 °C. FESEM, FT-IR, TGA, XRD, TEM, EDX, PL and UV–Vis were applied to study the formation of as-prepared nanoparticles and their structure, shape, elemental composition and optical characteristics. Moreover, the photocatalytic characteristics of as-synthesized praseodymium oxide were examined by photodegradation of β-naphthol under UV light illumination.

1 Introduction

In recent years, considerable attention has been focused on nanostructured materials due to their wide range of special applications and interesting characteristics [1–5]. Pr$_6$O$_{11}$ with oxygen-deficient modified fluorite structure is one of the most considerable rare earth metal oxides with interesting and particular optical and electrical characteristics, and has been studied widely for potential technological applications in organic light emitting diode as phosphors, materials with higher electrical conductivity as semiconducting oxide, ceramic pigments, three way catalyst as promoter, combustion catalysts as stabilizer, and catalysts [6–11]. Very limited numbers of methods including molten salt [12], electrochemical [13], hydrothermal [14], thermal decomposition [15], electrospinning [16], and precipitation [17] are available for the synthesis of the Pr$_6$O$_{11}$ nanostructures.

It is generally accepted that the size and morphology has a key impact on the behavior and application of the nanostructured materials. So, different approaches are proposing to optimize and control the shape and particle size of nanostructured materials. The synthesis of nanostructured metal oxides via thermal decomposition of organometallic complexes with specific architecture way is known as convenient, reliable and applicable approach owing to the easy controlling of the reaction conditions, shape, particle size and purity [18, 19].

Herein, nanocrystalline praseodymium oxide was prepared through thermal decomposition of praseodymium source ([PrL(NO$_3$)$_2$]NO$_3$ (L = (N,N′-bis(2′-hydroxyace-tophenonimine)-o-dipropylene triamin). Thermal decomposition of the praseodymium source was carried out in at various temperatures in the 300–800 °C. Saving time and energy, easy and mild preparation conditions and free surfactant cause introducing this way as simple, safe and efficient approach.

2 Experimental

2.1 Materials and characterization

Nanocrystalline praseodymium oxide and the PS were synthesized, utilizing the following chemicals, purchased

✉ Masoud Salavati-Niasari
  salavati@kashanu.ac.ir

[1] Institute of Nano Science and Nano Technology, University of Kashan, P. O. Box 87317-51167, Kashan, Islamic Republic of Iran

from Merck Co KG aA, Darmstadt, Germany: methanol, praseodymium nitrate ($Pr(NO_3)_3 \cdot 6H_2O$), 2′-hydroxyace-tophenone, chloroform, dipropylene triamin and ethyl acetate. Fourier transform infrared spectra of the as-synthesized samples were obtained utilizing KBr pellets on a FT-IR spectrometer (Thermo Nicolet Magna-IR 560 spectroscopy; Madison, WI) in the 400–4000 cm^{-1} range. FESEM images of as-prepared samples were visualized by a Tescan mira3 Czech field emission scanning electron microscope (FESEM; Brno, Czech). Powder X-ray diffraction (XRD) pattern of the as-obtained Pr_6O_{11} was obtained utilizing a diffractometer of Philips Company (Nagoya, Japan) with X'PertPro monochromatized Cu Ka radiation (l = 1.54 Å). Thermogravimetric-differential thermal analysis (TG–DTA) was performed applying a Shimadzu TGA-50 H Japan thermal gravimetric analysis instrument with a heating rate of 10 °C min^{-1} (TG–DTA; Kyoto, Japan). The energy dispersive spectrometry (EDS) analysis of the as-prepared Pr_6O_{11} was examined by XL30, Philips microscope (Eindhoven, the Netherlands). Transmission electron microscope (TEM) images of the as-synthesized Pr_6O_{11} were recorded on a JEM-2100 (Boston, MA) with an accelerating voltage of 200 kV equipped. A Perkin Elmer (LS55; Shelton, CT) fluorescence spectrophotometer was applied to study room temperature photoluminescence (PL) of the as-obtained Pr_6O_{11}. The electronic spectrum of the as-prepared Pr_6O_{11} was taken on a Scinco UV–Vis scanning spectrometer (Model S-4100, Scinco, Daejeon, South Korea).

2.2 Preparation of the compound (L)

For synthesizing of the N,N′-bis(2′-hydroxyacetophenon-imine)-o-dipropylene triamin compound (L), a stoichiometric amount of 2′-hydroxyacetophenone (0.02 mol) dissolved in methanol (25 cm^3) was added drop-wise to a dipropylene triamin solution (0.01 mol) in 25 cm^3 of methanol. A yellow precipitate of the Schiff-base compound (L) was obtained after refluxing the mixture for 3 h, separating by filtering, washing and air-drying. It was finally recrystallized from methanol.

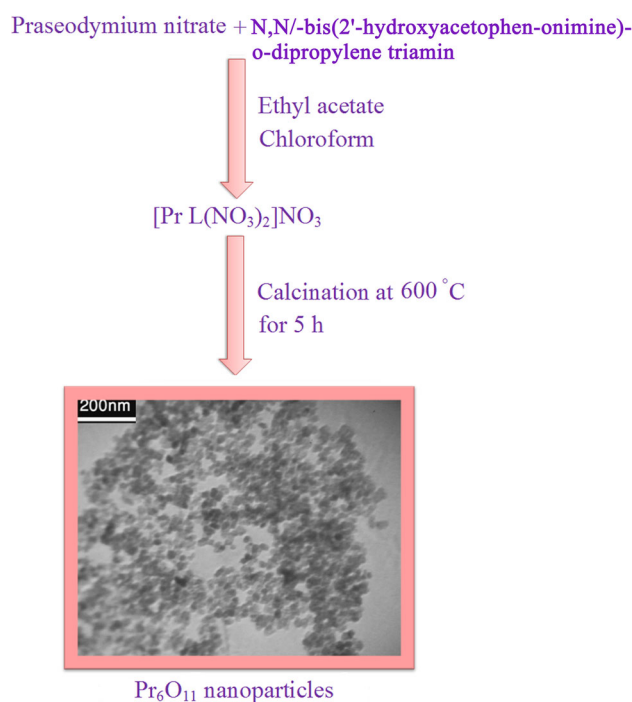## 2.3 Preparation of the praseodymium source (PS)

For synthesizing of the PS, 1 mmol praseodymium nitrate was dissolved in 12 cm^3 ethyl acetate and then was drop-wise to a solution of 1 mmol compound L in 12 cm^3 chloroform. The mixture was stirred for 2 h. Then, the yellow precipitate was filtered, washed with ethyl acetate and chloroform for three times, and after that air-dried for 24 h at room temperature.

2.4 Preparation of nanocrystalline praseodymium oxide

For synthesizing of the praseodymium oxide nanoparticles, 0.15 g of the as-obtained PS was subjected to thermal treatment at 600 °C for 5 h. The temperature reached to 600 °C by the 30 °C/min rate. And after 5 h, it was allowed to decrease to room temperature. Figure 1 illustrates the Schematic diagram of the preparing of Pr_6O_{11} nanoparticles. For studying the influence of calcination temperature, the thermal decomposition of the PS was carried out in the 300, 400, 500, 700 and 800 °C. For investigating, the effect of L, a blank sample was prepared. The blank sample was synthesize by subjecting the 0.15 g of $Pr(NO_3)_3 \cdot 6H_2O$ to thermal treatment at 600 °C. Table 1 exhibits the preparation conditions of Pr_6O_{11}. In order to characterize the as-prepared Pr_6O_{11}, techniques like EDS, PL, XRD, SEM, FT-IR, TEM and UV–Vis were utilized.

2.5 Photocatalytic test
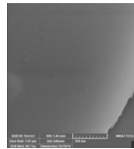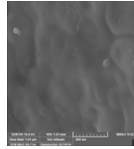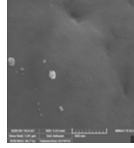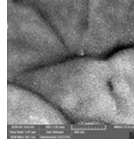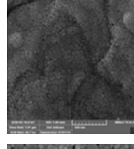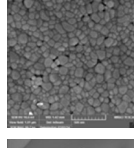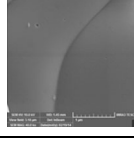
The photocatalytic characteristics of as-synthesized praseodymium oxide nanoparticles were evaluated by utilizing β-naphthol solution. The Solution including the 0.001 g of the β-naphthol and 0.05 g of the as-obtained praseodymium oxide in the quartz reactor was utilized to perform the photocatalytic test. After aerating for 30 min, the mixture was subjected to the irradiation of the UV light

Praseodymium nitrate + N,N/-bis(2′-hydroxyacetophen-onimine)-o-dipropylene triamin

Ethyl acetate
Chloroform

$[Pr L(NO_3)_2]NO_3$

Calcination at 600 °C
for 5 h

200nm

Pr_6O_{11} nanoparticles

Fig. 1 Schematic diagram of the Pr_6O_{11} nanoparticles preparation

Table 1 Preparation conditions of products

Sample no.	Precursor	Calcination temperature (°C)	SEM
1	PS	300	
2	PS	400	
3	PS	500	
4	PS	600	
5	PS	700	
6	PS	800	
7[a]	$Pr(NO_3)_3 \cdot 6H_2O$	600	

[a] Blank test, in the absence of (L) compound

from the 400 W mercury lamps. The β-naphthol photodegradation percentage was estimated as follow:

$$D.P. \,(t) = \frac{A_0 - A_t}{A_0} \times 100 \qquad (1)$$

where A_t and A_0 are the obtained absorbance value of β-naphthol solution at t and 0 min by a UV–Vis spectrometer, respectively.

3 Results and discussion

## 3.1 Structural properties of L compound, PS and praseodymium oxide

As mentioned before, in this work the $([PrL(NO_3)_2]NO_3$ (L = (N,N'-bis(2′-hydroxyacetophenonimine)-o-

dipropylene triamin) prepared and applied in the praseodymium oxide synthesis. To determine the (L) compound, PS and praseodymium oxide formation, FT-IR analysis was carried out. Figure 2a exhibits the FT-IR spectrum of the (L) compound. The bands located at 1610 and 1263 cm^{-1} are attributable to the v(C=N) and v(Ar–O), respectively (Fig. 2a) [19]. The FT-IR spectrum of PS shows the (L) compound characteristic bands with various shifts owing to PS preparation. An increase in the C–O stretching frequency (12 cm^{-1}) compared to the free (L) compound are seen in the FT-IR spectrum of the PS (Fig. 2b). This increase in the frequency demonstrates that the (L) compound coordinated to the praseodymium ion by means of the hydroxyl benzene oxygen atoms [20]. Furthermore, the band centered at 573 cm^{-1} in Fig. 2b which
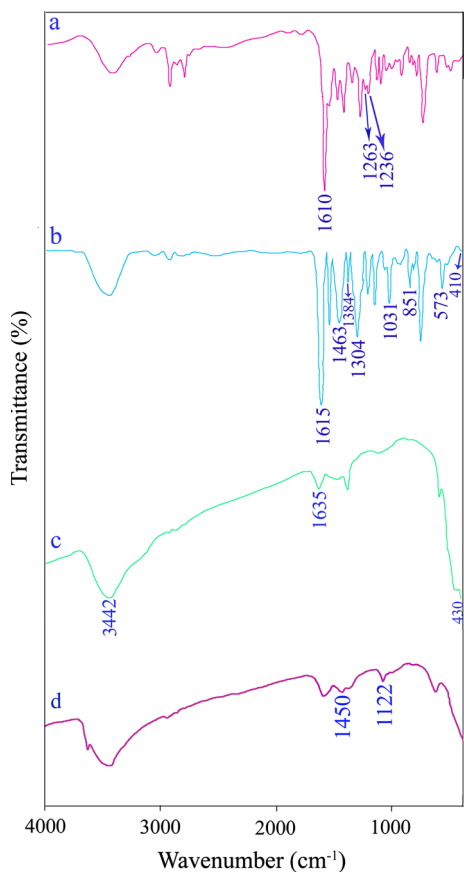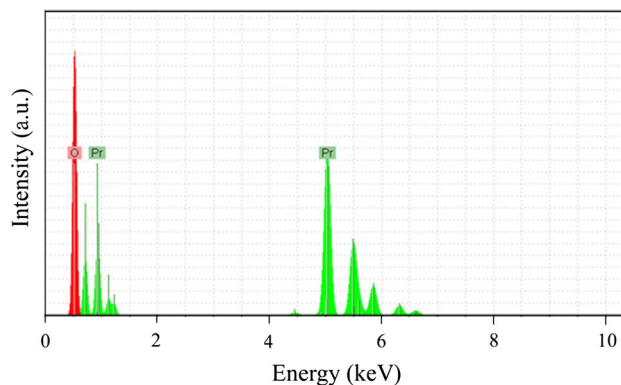
Fig. 2 FT-IR spectra of (*a*) compound (L), (*b*) PS, and Pr_6O_{11} nanoparticles obtained upon thermal treatment of the PS at 600 °C before (*c*) and after (*d*) photocatalytic treatment
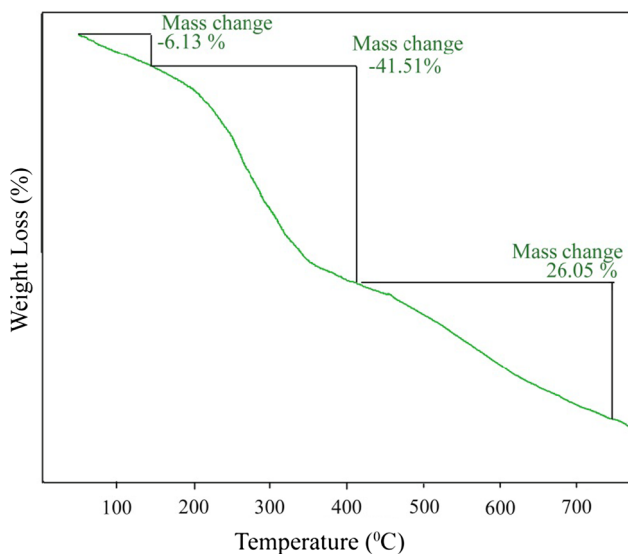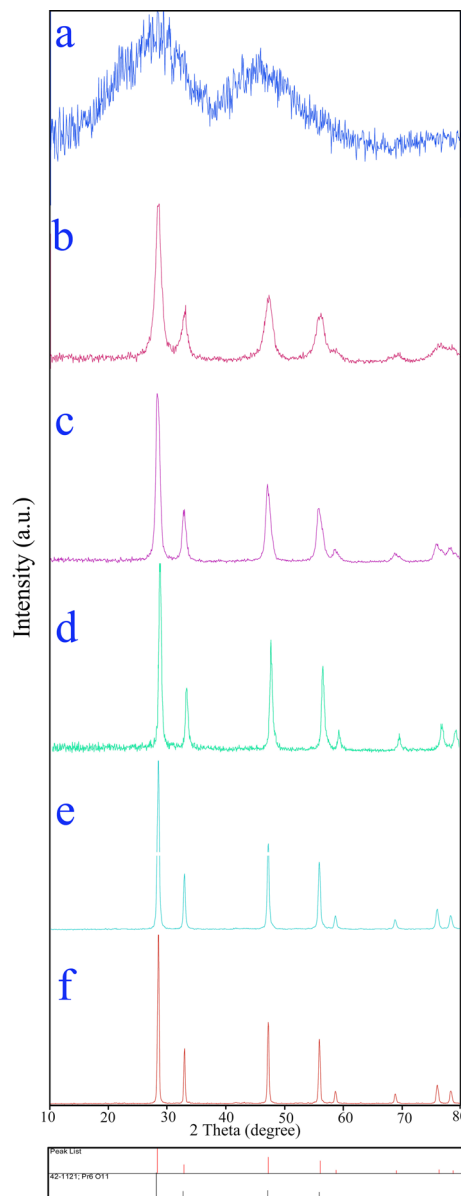
Fig. 4 XRD patterns of the Pr_6O_{11} samples obtained by thermal treatment of PS at 300 (*a*), 400 (*b*), 500 (*c*), 600 (*d*), 700 (*e*) and 800 °C (*f*)

Fig. 3 TGA of the PS

Fig. 5 EDS pattern of Pr_6O_{11} nanoparticles synthesized at 600 °C

can be ascribed to v(Pr–O) vibration, proved this coordination mode [21]. The v(C=N) band in the PS shifted to 1615 cm^{-1}. A stronger characteristic of the iminic bonds as well as azomethines nitrogen atoms contribution in the coordination mode demonstrated by this occurred blue shift (5 cm^{-1}) [19, 20]. Moreover, the peak centered at 410 cm^{-1} in Fig. 2b which might be ascribed to v(Pr–N) vibration, confirm this occurred coordination mode [21]. It is generally accepted that the differences in the two bands $|v_4 - v_1|$ detects the different nitrate groups coordination modes to the praseodymium metal. Several peaks centered at 1463 cm^{-1} (v_1), 1031 cm^{-1} (v_2), 851 cm^{-1} (v_3) and 1304 cm^{-1} (v_4) in the Fig. 2b ascribed to the coordinated nitrate ions [21]. The coordination mode of the NO$_3^-$ ions (as a bidentate compound) in the PS demonstrated by the observed difference between v_4 and v_1 (nearly 159 cm^{-1}) [22, 23]. The peak centered at 1385 cm^{-1} in the Fig. 2b ascribed to the (v_o) free nitrate [21]. In Fig. 2c, the peaks centered at 3442 and 1635 cm^{-1} are related to the v(OH) stretching and bending vibrations, which demonstrates that

physisorbed water molecules linked to as-obtained praseodymium oxide [23]. The characteristic band for Pr–O vibration (Fig. 2c) is observed at 430 cm^{-1} [24]. As can be seen, FT-IR results demonstrate the (L) compound, PS and praseodymium oxide preparation.

3.2 Thermal gravimetric analysis (TGA) of the PS

Thermal gravimetric technique (TGA) was applied to investigate the thermal stability of the as-synthesized PS. The TGA curve of the as-prepared PS is shown in Fig. 3. It can be observed that three mass loss steps occurred. The occurred mass loss in the 60–150 °C (showing 6.13 % mass loss) corresponds to the removal of the surface moisture. The happened step at the 150–400 °C (indicating 41.51 % mass loss) corresponds to the removal of the (L) compound. The happened step in the 400–750 °C (indicating 26.05 % mass loss) corresponds to the removal of the nitrate species from the coordination sphere of the as-prepared PS, and the preparation of Pr$_6$O$_{11}$.

Fig. 6 SEM images of the products prepared at **a** 300, **b** 400 and **c** 500 °C
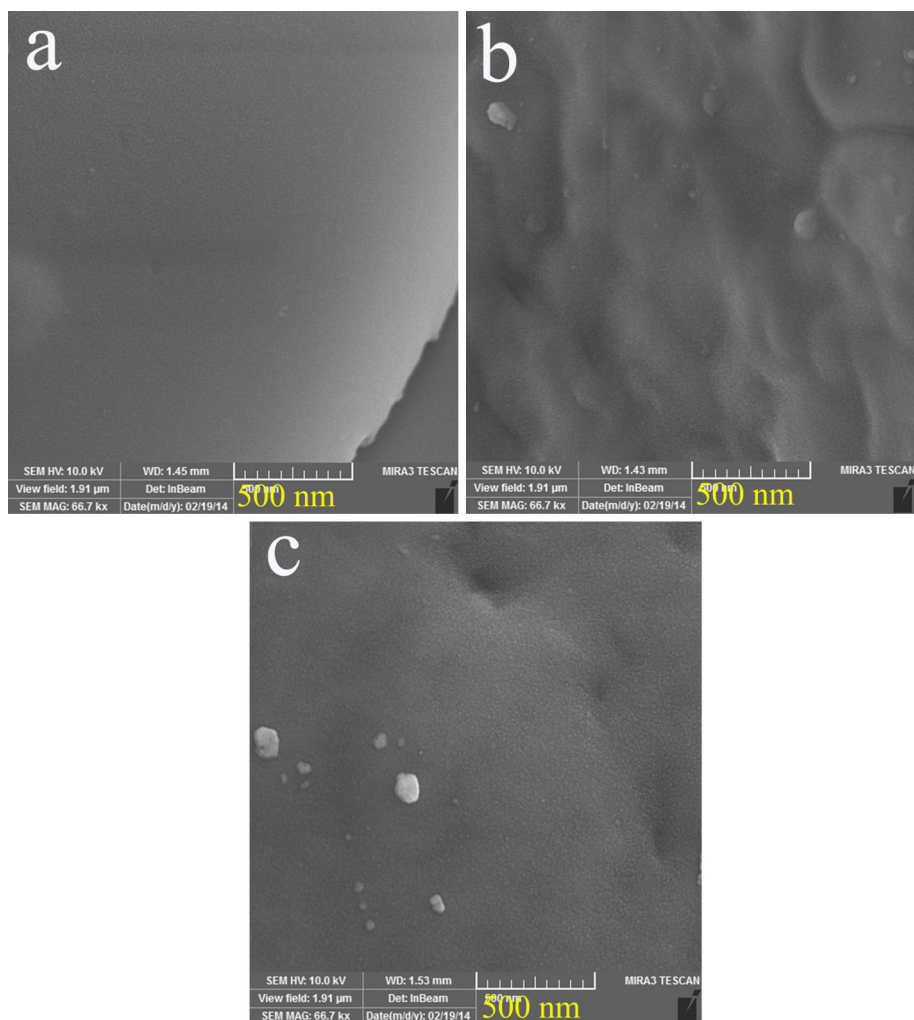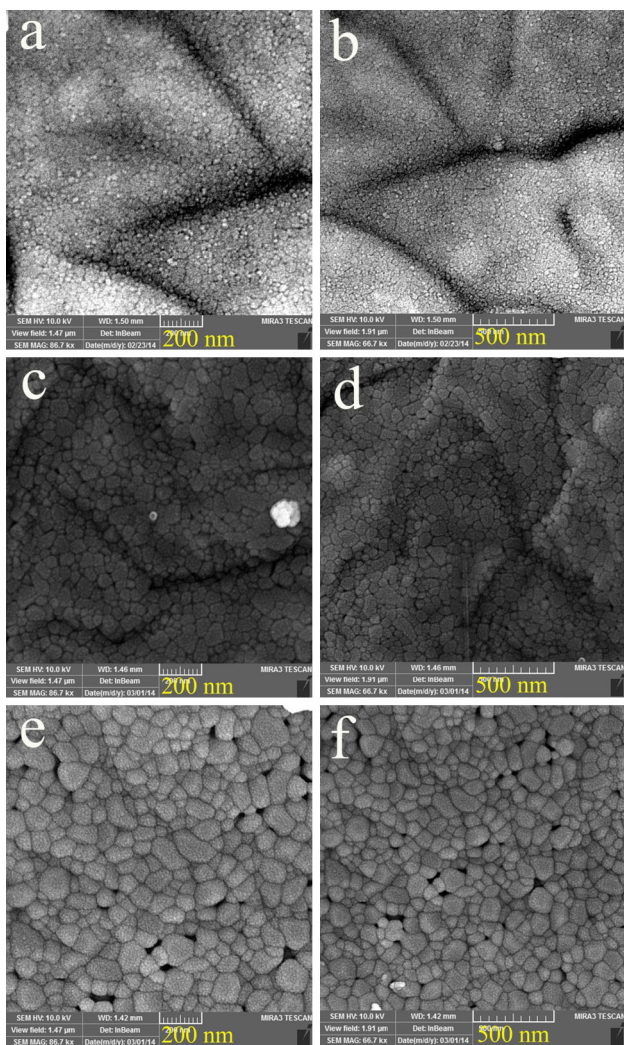
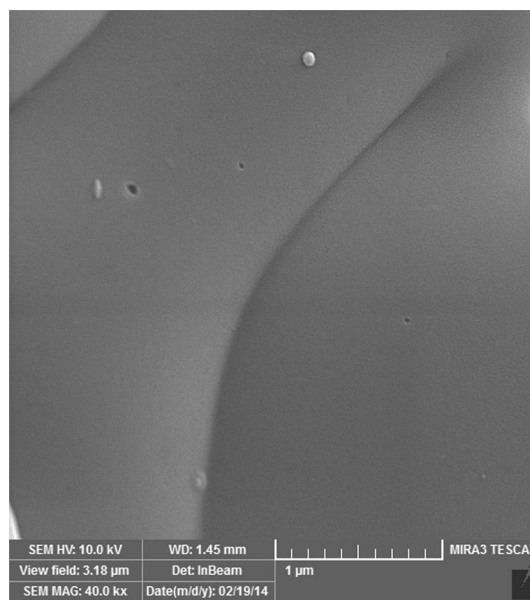**Fig. 7** SEM images of the samples synthesized at **a**, **b** 600, **c**, **d** 700 and **e**, **f** 800 °C

Fig. 8 SEM images of sample prepared in the absence of (L) compound

3.3 Pr_6O_{11} XRD and EDS analyses

XRD analysis was performed to determine the composition and crystal structure of the samples. The XRD patterns illustrated in Fig. 4a–f correspond to the samples obtained by thermal treatment of PS at 300, 400, 500, 600, 700 and 800 °C, respectively. As illustrated in Fig. 4a, the sample prepared at 300 °C seems amorphous. By increasing the temperature from 300 to 800 °C, pure Pr_6O_{11} has been formed (Fig. 4b–f). The crystallite sizes of the Pr_6O_{11} samples prepared at 400, 500, 600, 700 and 800 °C calculated by the Scherrer equation [24] are 11.5, 14.8, 16, 26 and 34.7 nm, respectively. These results demonstrate that the crystallite size of Pr_6O_{11} enhances by changing the temperature from 400 to 800 °C. To further confirm the purity and chemical composition of the as-prepared Pr_6O_{11}, EDS analysis was employed. In the EDS spectrum of
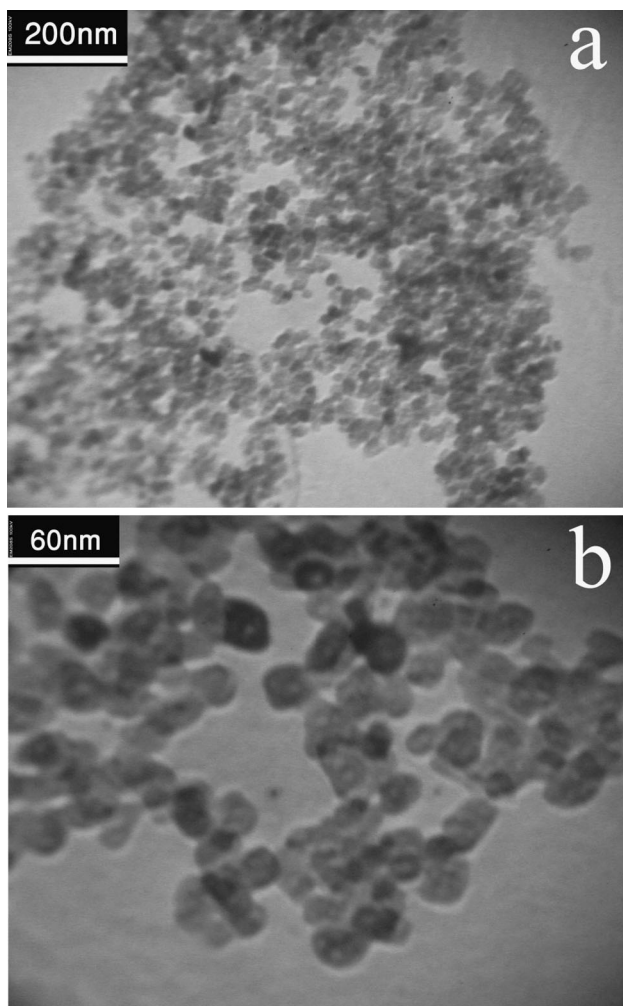
sample no. 4 (Fig. 5), Pr and O elements are detected. So, both XRD and EDX analyses demonstrate that pure praseodymium oxide nanoparticles were successfully produced via the present synthetic way.

3.4 Pr_6O_{11} FESEM and TEM analyses

In order to investigate the calcination temperature influence on the particle size and shape of the Pr_6O_{11}, SEM images of PS calcined at 300, 400, 500, 600, 700 and 800 °C were taken and illustrated in Figs. 6 and 7, respectively. Obviously (Fig. 6a), 300 °C is not the needed temperature for decomposition of PS. The sample nos. 2 and 3 obtained at 400 and 500 °C show high agglomerated tiny particle-like structures (Fig. 6b, c). It seems that when calcination temperature increases from 500 to 600 °C, the kinetic energy increases and particles agglomerate and therefore nanoparticles with very uniform sphere-like shape (sample no. 4) are prepared at 600 °C (Fig. 7a, b). By increasing the calcination temperature from 600 to 800 °C, more kinetic energy increases and nanoparticles more agglomerate, and therefore the grain size of particles becomes larger and the amount of spherical and uniform Pr_6O_{11} nanoparticles decreases. So the thermal decomposition temperature plays an important role to control particle size and shape of Pr_6O_{11}.

The influence of the (L) compound was studied by preparing the sample no. 7 as blank product without employing any (L) compound at 600 °C. SEM image of blank product is illustrated in Fig. 8. It is noteworthy that bulk structures were produced. This result proved
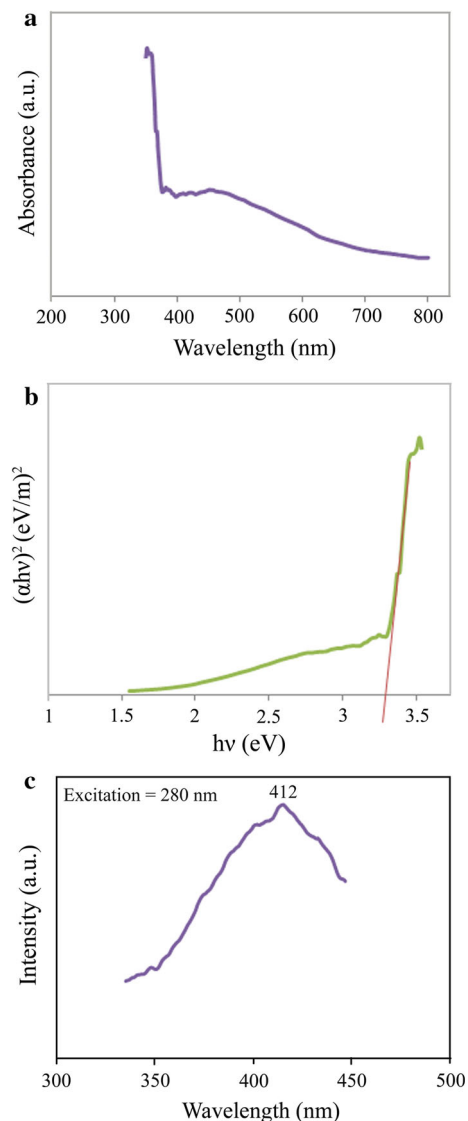
Fig. 9 TEM images of Pr_6O_{11} nanoparticles synthesized at 600 °C

Fig. 10 UV–Vis diffuse reflectance spectrum (**a**), plot to determine the band gap (**b**) and PL spectrum (**b**) of the Pr_6O_{11} prepared at 600 °C

employing (L) compound with high steric hindrance effect cause to produce nanoparticles with very uniform sphere-like shape (sample no. 4) with small grain size at 600 °C, and therefore compound with the huge size may be employed instead of general stabilizers to control the shape and size.

TEM analysis was carried out to investigate the detailed shape and particle size. Figure 9a and b shows TEM image of Pr_6O_{11} synthesized at 600 °C, indicating uniform sphere-like shape with a mean size of about 20 nm. The presence of uniform nanoparticles with narrow size distribution proved by a TEM image that is illustrated shape and particle size.

3.5 Optical properties of Pr_6O_{11}

UV–Vis diffuse reflectance and PL analyses were performed to characterize the optical properties of as-prepared Pr_6O_{11}. The UV–Vis diffuse reflectance spectrum of
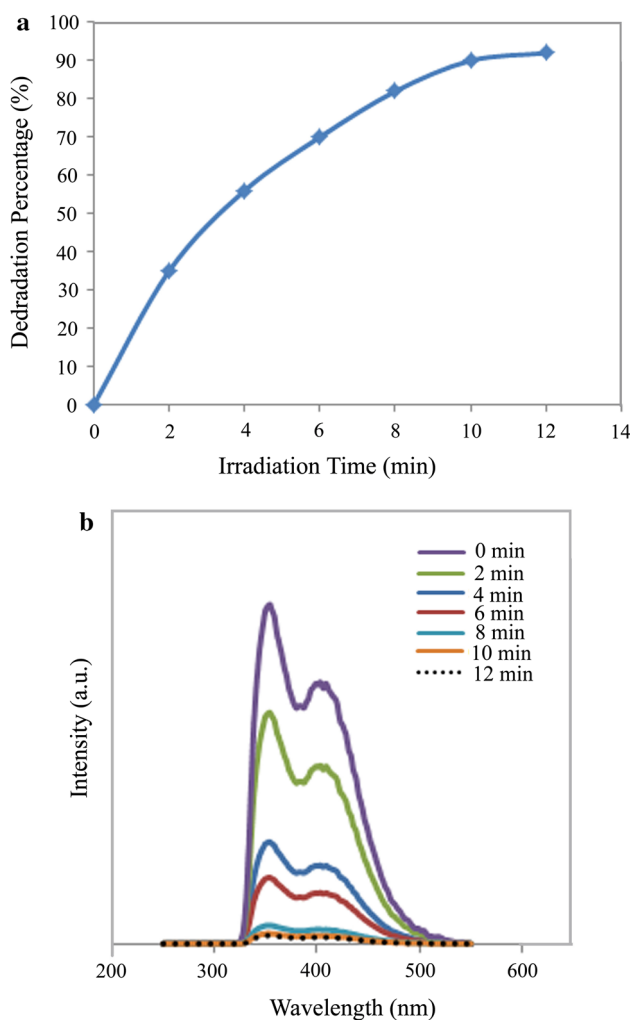
Pr_6O_{11} nanoparticles obtained by the calcination of PS at 600 °C is seen in Fig. 10a. It shows absorption peak at 352 nm. It is well known that the band gap (E_g) plays a significant role in characterizing the properties of nanostructured materials applied in photocatalytic processes. The (E_g) can be evaluated based on the absorption spectrum using Tauc's relationship [25]:
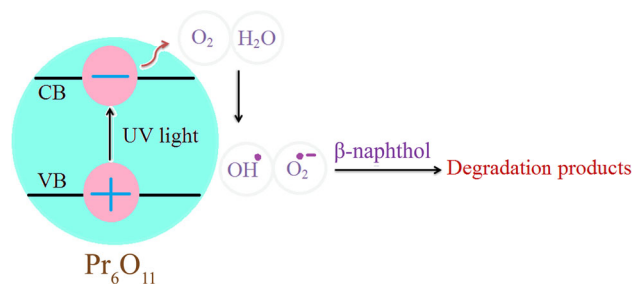
$$(Ahv)^n = B(hv - E_g) \qquad (2)$$

where, hv is the photo energy, A is absorbance amount, B is a material constant and n is 2 or 1/2 for direct and indirect transitions. The energy gap (E_g) of the Pr_6O_{11} as direct semiconductor was obtained by extrapolating the linear portion of the plot of $(\alpha hv)^2$ against hv to the energy axis

Fig. 12 Reaction mechanism of β-naphthol photodegradation over praseodymium oxide nanoparticles under UV light illumination

3.6 Photocatalytic properties of Pr_6O_{11}

The photocatalytic characteristics of as-obtained Pr_6O_{11} nanoparticles (sample no. 4) were evaluated by the degradation of β-naphthol solution under UV light (Figs. 11, 12). Without UV light or as-prepared nanoparticles, practically no β-naphthol was break down after 12 min, revealing the insignificant contribution of self-degradation. According to photocatalytic calculations by Eq. (1), the β-naphthol degradation was about 92 % after 12 min illumination of UV light, and as-prepared Pr_6O_{11} nanoparticles demonstrated very well photocatalytic activity. Figure 11b presents the spectrofluorimetric time-scans of β-naphthol solution with Pr_6O_{11} nanoparticles. As seen in Fig. 11b, the removal of β-naphthol on the praseodymium oxide under UV light seems continuous. Moreover, FT-IR spectrum of the Pr_6O_{11} nanoparticles (sample 4) after photocatalytic treatment is illustrated in Fig. 2d. In this spectrum the weak peaks at 1450 and 1122 cm^{-1} are attributable to the aromatic ring stretching vibrations and C–H bonds bending vibrations [27], respectively, which indicates the presence of the very little β-naphthol on the surface of the Pr_6O_{11} nanoparticles after photocatalytic treatment. This obtained FT-IR result also confirms very well photocatalytic activity of the as-prepared Pr_6O_{11} nanoparticles. It is generally accepted that the heterogeneous photocatalytic processes comprise diffusion, adsorption and reaction steps, and suitable distribution of the pore is effective and useful to diffusion of reactants and products, which prefer the photocatalytic reaction. In this

Fig. 11 Photocatalytic β-naphthol degradation of Pr_6O_{11} nanoparticles synthesized at 600 °C under UV light (**a**) and fluorescence spectral time scan of β-naphthol irradiated at 365 nm with Pr_6O_{11} (**b**)

(Fig. 10b). The E_g amount of the Pr_6O_{11} determined to be 3.3 eV.

The PL spectrum of the sample no. 4 is illustrated in Fig. 10c. The excitation wavelength was 280 nm. It shows an emission peak at around 412 nm. This emission peak is attributed to charge transition from the $4f$ band to the valence band of praseodymium oxide nanoparticles, which is similar to the previous literatures [26].

Table 2 Characterization comparison of Pr_6O_{11} nanoparticles with other similar works

Method	Precursors	Crystallite size (nm)	Calcination temperature (°C)	References
Thermal treatment	[Pr L(NO$_3$)$_2$]NO$_3$ (L = N,N'-bis (2'-hydroxyacetophenonimine)-o-dipropylene triamin)	16	600	This work
Thermal decomposition	Praseodymium acetate (Pr(CH$_3$COO)$_3$·H$_2$O)	30	700	[29]
Thermal decomposition	Praseodymium acetate (Pr(CH$_3$COO)$_3$·H$_2$O)	Not reported	700	[15]
Thermal decomposition	Pr–citric acid complex	Not reported	1000	[30]
Thermal decomposition	Pr$_2$(CO$_3$)·8H$_2$O	Not reported	1000	[30]

investigation, the very well photocatalytic activity can be related to appropriate distribution of the pore, high hydroxyl amount and high separation rate of charge carriers [28–35].

For preparing the nanostructured materials via thermal treatment way, the choice of precursor plays a significant role. In this study compared to other reports, for the synthesis of Pr_6O_{11} via a surfactant-free thermal treatment route, $PrL(NO_3)_2]NO_3$ (L = N,N'-bis(2′-hydroxyacetophenonimine)-o-dipropylene triamin) as PS was used. N,N'-bis(2′-hydroxyacetophenonimine)-o-dipropylene triamin compound as complexing agent has high steric hindrance influence and is an appropriate capping agent for preparing of nanostructured Pr_6O_{11}. It seems that Schiff-base compound owing to its high steric hindrance influence causes nucleation to be happened rather than the growth. In Table 2 some of the precursors applied in other works are compared with the present study. According to these results, by thermal treatment of $[PrL(NO_3)_2]NO_3$, Pr_6O_{11}- was prepared successfully at lowest temperature.

4 Conclusion

In summary, this work has demonstrated the synthesis of nanocrystalline praseodymium oxide from the $[PrL(NO_3)_2]NO_3$ (L = N,N'-bis(2′-hydroxyacetophenonimine)-o-dipropylene triamin) as praseodymium source (PS) via a simple and surfactant-free thermal decomposition process. For studying the influence of calcination temperature, the thermal decomposition of the PS was carried out in at various temperatures in the 300–800 °C. Based on the results of this investigation, it was found that praseodymium oxide with very uniform sphere-like shape, small grain size and pure cubic phase could be synthesized by thermal decomposition of the obtained praseodymium source at 600 °C. The proposed way for the preparation of Pr_6O_{11} nanoparticles is cost effective, reproducible and convenient, which makes it very appropriate for large-scale production. Several techniques such as FESEM, TEM, XRD, UV–Vis, PL, FT-IR, and EDS were utilized to characterize the as-prepared nanoparticles properties. When as-prepared Pr_6O_{11} was employed as photocatalyst, the percentage of β-naphthol photodegradation was about 92 % after 12 min illumination of UV light. This result suggests that as-obtained Pr_6O_{11} nanoparticles as desirable material has great potential to be employed for photocatalytic applications under UV light.

References

1. S. Zinatloo-Ajabshir, M. Salavati-Niasari, J. Ind. Eng. Chem. **20**, 3313 (2014)
2. A. Sobhani, M. Salavati-Niasari, Mater. Res. Bull. **47**, 1905 (2012)
3. S. Zinatloo-Ajabshir, M. Salavati-Niasari, Int. J. Appl. Ceram. Technol. **11**, 654 (2014)
4. M. Salavati-Niasari, A. Khansari, F. Davar, Inorg. Chim. Acta **362**, 4937 (2009)
5. S. Zinatloo-Ajabshir, M. Salavati-Niasari, Ceram. Int. **41**, 567 (2015)
6. S. Bernal, F.J. Botana, G. Cifredo, J.J. Calvino, A. Jobacho, J.M. Rodriguez-Izquierdo, J. Alloys Compd. **180**, 271 (1992)
7. P. Šulcová, J. Therm. Anal. Calorim. **82**, 51 (2005)
8. S. Shrestha, C.M.Y. Yeung, C. Nunnerley, S.C. Tsang, Sens. Actuators, A **136**, 191 (2007)
9. K. Asami, K. Kusakabe, N. Ashi, Y. Ohtsuka, Appl. Catal. A Gen. **156**, 43 (1997)
10. M. Kawabe, H. Ono, T. Sano, M. Tsuji, Y. Tamaura, Energy **22**, 1049 (1997)
11. Bahaa M. Abu-Zied, Youssef A. Mohamed, Abdullah M. Asiri, J. Rare Earth **31**, 701 (2013)
12. X. Wang, J. Zhuang, Y. Li, Eur. J. Inorg. Chem. **5**, 946 (2004)
13. X. Sun, T. Zhai, X. Lu, Sh Xie, P. Zhang, Ch. Wang, W. Zhao, P. Liu, Y. Tong, Mater. Res. Bull. **47**, 1783 (2012)
14. Y. Zhang, K. Han, X. Yin, Zh Fang, Zh Xu, W. Zhu, J. Cryst. Growth **311**, 3883 (2009)
15. Basma A.A. Balboul, J. Anal. Appl. Pyrol. **88**, 192 (2010)
16. M. Shamshi Hassan, Y.-S. Kang, B.-S. Kim, I.-S. Kim, H.-Y. Kim, M.-S. Khil, Superlattice Microst **50**, 139 (2011)
17. M. Salavati-Niasari, N. Mir, F. Davar, J. Phys. Chem. Solids **70**, 847 (2009)
18. M. Shakouri-Arania, M. Salavati-Niasari, New J. Chem. **38**, 1179 (2014)
19. T.A. Youssef, J. Coord. Chem. **61**, 816 (2008)
20. W.B. Sun, P.F. Yan, G.M. Li, H. Xu, J.W. Zhang, J. Solid State Chem. **182**, 381 (2009)
21. Z.A. Taha, A.M. Ajlouni, KhA Al-Hassan, A.K. Hijazi, A.B. Faiq, Spectrochim. Acta A **81**, 317 (2011)
22. W. Wang, Y. Huang, N. Tang, Spectrochim. Acta A **66**, 1058 (2007)
23. Y.L. Zhang, W.W. Qin, W.S. Liu, M.Y. Tan, N. Tang, Spectrochim. Acta A **58**, 2153 (2002)
24. R.L. Snyder Jenkins, *Chemical Analysis: Introduction to X-Ray Powder Diffractometry* (Wiley, New York, 1996), pp. 89–91
25. M. Salavati-Niasari, D. Ghanbari, M.R. Loghman-Estarki, Polyhedron **35**, 149 (2012)
26. N. Krishna Chandar, R. Jayavel, Mater. Res. Bull. **50**, 417 (2014)
27. S. Weng, Z.X. Pei, Z. Zheng, J. Hu, P. Liu, A.C.S. Appl, Mater. Interfaces **5**, 12380 (2013)
28. J. Zhong, J. Li, F. Feng, Y. Lu, J. Zeng, W. Hu, Z. Tang, J. Mol. Catal. A: Chem. **357**, 101 (2012)
29. B.M. Abu-Zied, S.A. Soliman, Thermochim. Acta **470**, 91 (2008)
30. M. Popa, M. Kakihana, Solid State Ionics **141–142**, 265 (2001)
31. D. Ghanbari, M. Salavati-Niasari, S. Karimzadeh, S. Gholamrezaei, J. Nanostruct. **4**, 227 (2014)
32. G. Nabiyouni, S. Sharifi, D. Ghanbari, M. Salavati-Niasari, J. Nanostruct. **4**, 317 (2014)
33. M. Panahi-Kalamuei, M. Mousavi-Kamazani, M. Salavati-Niasari, J. Nanostruct. **4**, 459 (2014)
34. F. Beshkar, M. Salavati-Niasari, J. Nanostruct. **5**, 17 (2015)
35. L. Nejati-Moghadam, A. Esmaeili Bafghi-Karimabad, M. Salavati-Niasari, H. Safardoust, J. Nanostruct. **5**, 47 (2015)